Supporting Information

The synergistically enhanced activity and stability of layered manganese oxide via engineering of defects and K^+ ions for oxygen electrocatalysis

Zihao Zhou,†[a] Xiaoying Zheng,†[a,c] Hongyun Huang,[a] Yanli Wu,[a] Shengbo Han,[a] Weixiong Cai,[a] Bang Lan,*[b] Ming Sun,*[a] and Lin Yu*[a]

[a] Key Laboratory of Clean Chemistry Technology of Guangdong Regular Higher Education Institutions, Guangdong Provincial Key Laboratory of Plant Resources Biorefinery, School of Chemical Engineering and Light Industry, Guangdong University of Technology, 510006 Guangzhou, P. R.China

[b] School of Chemistry and Environment, Jiaying University, 514015 Meizhou, P. R.China

[c] Institut National de la Recherche Scientifique (INRS), Énergie Matériaux Télécommunications (EMT), 1650, Boulevard Lionel-Boulet, Varennes (Québec) J3X 1P7, Canada

1 Experimental section

1.1 Characterization

The crystal structures of the four samples were investigated by X-ray powder diffraction (XRD) on a PANalytical X'Pert3 Powder X-ray Diffractometer operating with Cu target ($\lambda_{K\alpha}$ = 0.154 nm) and Raman spectra on a LabRAM HR Evolution spectrometer with a 633 nm excitation light source. To observe the morphology and obtain element mapping, scanning electron microscope (FE-SEM) and transmission electronic microscopy (FE-TEM) patterns were separately captured on a Hitachi SU8220 microscope (3.0 kV, 10.0 μA) and an FEI Thermo Talos F200S microscope (200 kV). The selected area electron diffraction (SAED) images and element mapping were collected during the TEM tests. The surface information was acquired using X-ray photoelectron spectroscopy (XPS, Thermo Fisher, Escalab 250Xi) with a 0.05 eV energy

step and a 40.0 eV pass energy.

1.2 Electrochemical measurements

The catalyst inks for ORR and OER were the mixtures of 3.5 mg catalyst, 1.5 mg ketjenblack conductive carbon, 750 μl ethanol, 250 μl deionized water, and 50 μl 5 wt% Nafion^{TM} solution. For the ink of commercial 20% Pt/C, the catalyst dosage was increased to 5 mg and no conductive carbon was required.

For the rechargeable zinc-air batteries, the inks of samples needed nothing to adjust based on that for ORR and OER. In contrast, that of precious metal catalysts is different. To realize the charging function, RuO_2 was added. Hence, the solid-state components in the ink were 5 mg 20% Pt/C, 3.5 mg RuO_2, and 1.5 mg ketjenblack conductive carbon.

A CHI 760E electrochemical workstation (Shanghai Chenhua Instruments Limited, China) was connected to a three-/four-electrode system, which was employed to carry out the electrochemical measurements. For OER, the three-electrode system was assembled with a working electrode (a carbon fiber paper (CFP)), a counter electrode (a graphite rod), and a revisionary Ag/AgCl (in 3.5 M KCl) reference electrode. For ORR, a rotating ring disk electrode (RRDE) was employed as the working electrode in a four-electrode system. All tests were carried out in the O_2-saturated KOH solution with various concentrations of 0.1 M for ORR and 1.0 M for OER.

For ORR, the as-prepared fresh inks were dripped on the disk of the RRDE with a mass loading of samples about 0.088 mg_{cat} cm^{-2}. The ORR properties were investigated via cyclic voltammetry (CV), linear sweep voltammetry (LSV), and chronoamperometry. Firstly, the inks were dripped onto the RRDE surface and dried form a uniform film. Secondly, to measure CV curves in a potential window from 0.27 to 1.17 V (vs. RHE) at a scan rate of 50 mV s^{-1}. Thirdly, set the rotating speed as 1600 rpm, and measured the LSV curves at 5 mV s^{-1} with a ring potential of 1.57 V (vs. RHE) in the same potential window. After that, stability was tested by the 12-hour

chronoamperometric curves with a rotating speed of 400 rpm and at 0.57 V vs. RHE. Furthermore, the stability was also tested by accelerated degeneration tests (ADT). It means that after a routine LSV scanning, a 1000-cycle special CV (0.67-0.87 V vs. RHE, 100 mV s^{-1}) and another routine LSV were separately conducted. The degeneration of the $E_{1/2}$ between the two LSV curves was used to access the stability of the samples.

For OER, the inks were dropped on carbon fiber paper (CFP) with a mass loading approximate to 0.300 mg_{cat} cm^{-2}. The OER activity was appraised by LSV curves in a potential window in the range from 1.13 to 1.83 V (vs. RHE) with a scan rate of 5 mV s^{-1}. The ECSA was collected by CV curves in the N_2-saturated 0.1 M KOH solution from 1.02 to 1.12 V (vs. RHE) with a series of scan rates (10, 20, 30, 40, 50 mV s^{-1}).

1.3 Fabrication and measurement of the rechargeable zinc-air battery

The rechargeable zinc-air battery employed a polymethyl methacrylate model with air-electrodes, 0.5 mm-thick zinc plates, and alkaline electrolytes. For the air-electrodes of rechargeable zinc-air battery, the air-electrode was a stainless-steel mesh coated one-side with a 0.2 mm polytetrafluoroethylene gas diffusion layer with the mass loading of 0.875 mg_{cat} cm^{-2} for the samples or 2.125 mg_{cat} cm^{-2} for the precious metal catalyst (0.875 mg_{cat} cm^{-2} for RuO_2 and 1.250 mg_{cat} cm^{-2} for 20% Pt/C). In detail, the effective area of an air-electrode was 1 cm^{-2} and the solutes in the electrolyte were 6.0 M KOH and 0.2 M $Zn(CH_3COO)_2$. The assembled rechargeable zinc-air batteries were tested on a CHI 760E electrochemical workstation and a LAND CT3001A 1U system. The open-circuit voltage and the polarization curves for power density were collected on the former, and the other tests were recorded on the latter. The LSV curves for power density were started at 1.6 V (vs. zinc) and ended at 0.2 V (vs. zinc) with a scan rate of 5 mV s^{-1}. The galvanostatic charge-discharge (GCD) was run under 5 mA cm^{-2} for 10 min per charge/discharge step until the batteries were out of action or cycled 1000 times. To determine the rate performance, the discharge curves were run following an alterable current density programming with a 60-min working time and a 2-min interval time per segment. The current densities were set

as 2, 5, 10, 20, 30, and 5 mA cm^{-2} per segment.

2 Figures and Tables

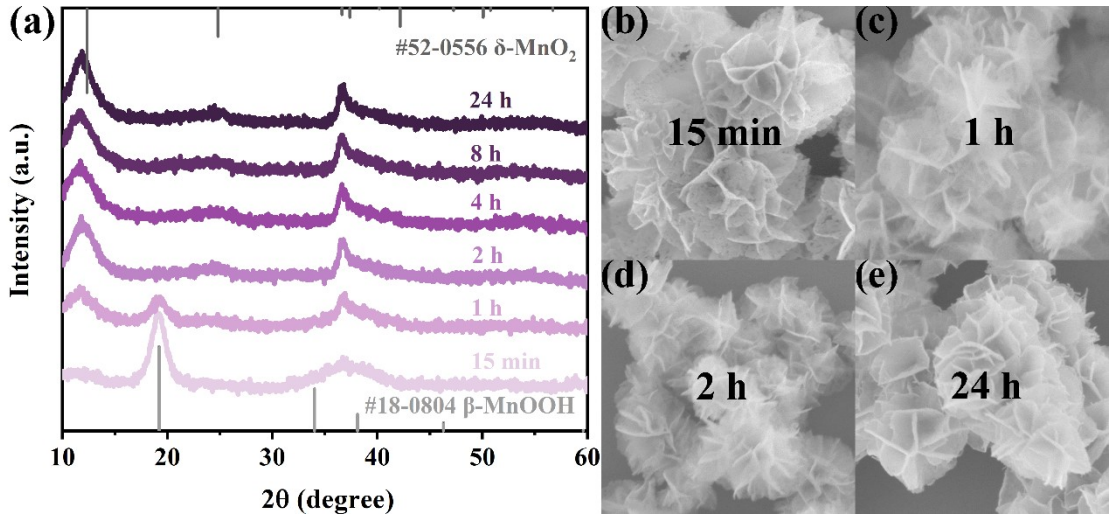

Fig.S1 (a) The XRD patterns and (b-e) the corresponding SEM images under different reaction times controlled the MnO_2 scheme.

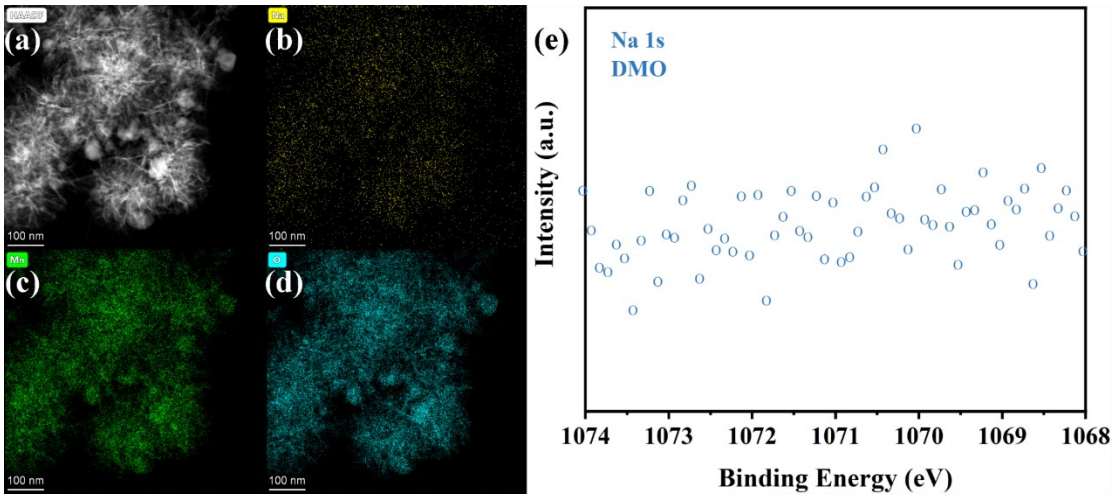

Fig.S2 (a) The element mapping and (b) the XPS of the Na 1s core level of the DMO.

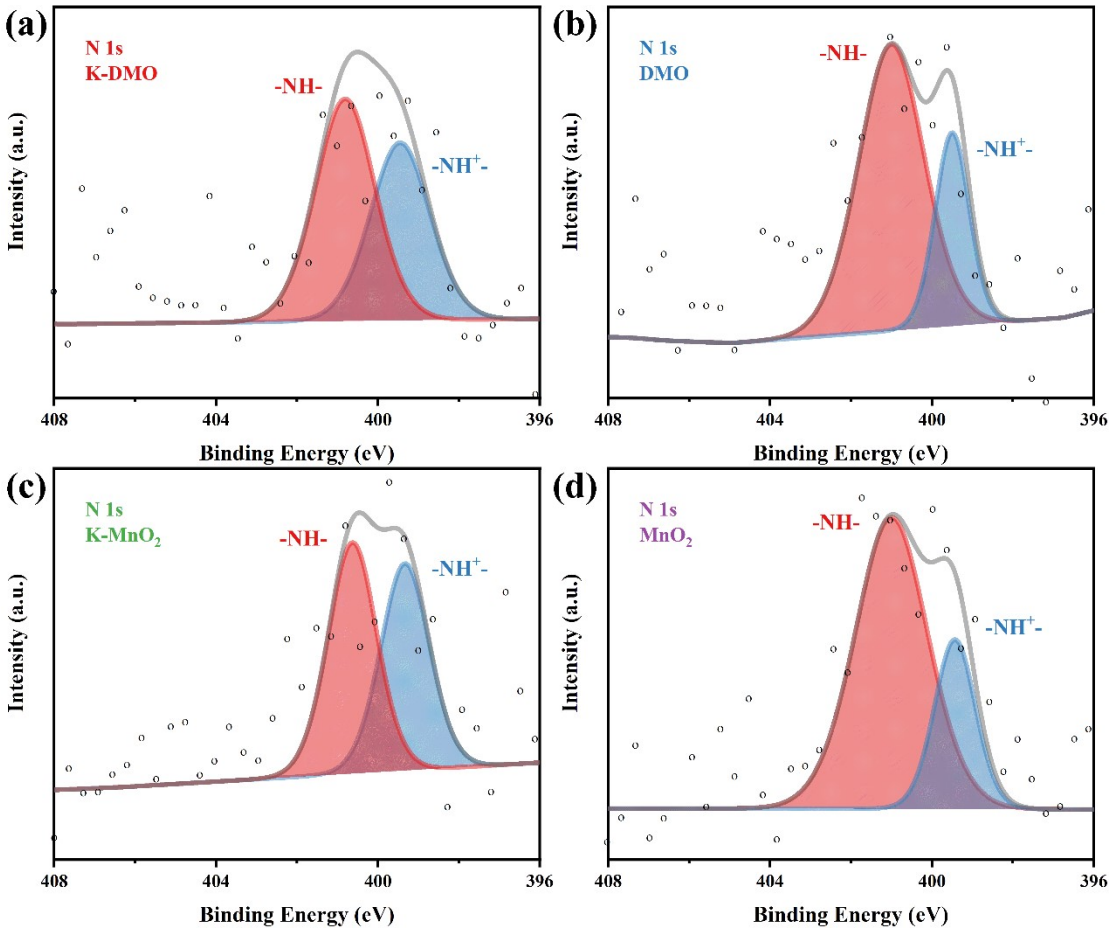

Fig.S3 The XPS of the N 1s region.

Fig.S3 shows the N 1s signal of the four samples. Two deconvolution peaks located at ~400.9 and ~399.4 eV are characteristic of -NH- and -NH^+- moieties.[1, 2] No signal indexed to NO_3^- is detected. Hence, it is reasonable to assert that the N element exists in NH_4^+ rather than NO_3^-.

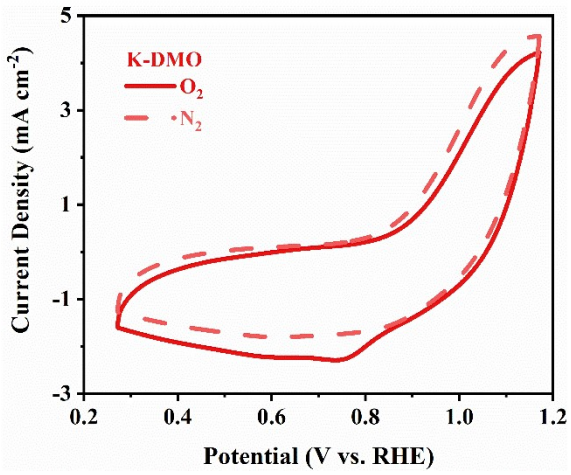

Fig.S4 The CV curves of the K-DMO sample measured in O_2-/N_2-saturated 0.1 M KOH solution

Table S1 The relative atomic content measured via EDX

Samples	K/Mn	Na/Mn	Mn (%)	O/Mn
K-DMO	0.07(4)	-	29.85	2.27(6)
DMO	-	0.01(4)	27.86	2.57(5)
K-MnO_2	0.06(8)	-	32.73	1.98(7)

Table S2 The relative atomic content measured via XPS

Samples	K (%)	Na (%)	N (%)	Mn (%)	O (%)
K-DMO	0.95	-	1.67	33.02	64.36
DMO	-	-	1.69	33.51	64.80
K-MnO_2	2.17	-	2.43	32.41	62.99
MnO_2	-	-	2.62	33.64	63.74

Table S3 The summary of ORR performance of MnO_2-based materials

Samples	$E_{1/2}$ (V vs. RHE)	j_L (mA cm^{-2})	Stability (%)	Reference
K-DMO	0.75	5.30	89.84 (12 h)	This work
MnO_x/C-D	0.82	5.47	90.0 (12 h)	3
MnO_2/Super P Li	0.76	~5.2	87 (10 h)	4
EDM	-	~2.7	-	5
Co-DEM	-	~2.7	-	5
MnO_2/C_{ZIF-67}	0.79	5.92	81 (11 h)	6
α-MnO_2	0.72	1.7	-	7
C-MnO_2	0.75	3.4	-	7
N-C/MnO_2/N-C	0.726	5.93	-	8
Co/MnO@NC	0.83	~6.6	90 (20 h)	9

Table S4 The summary of zinc-air battery performance with MnO_2-based materials

Samples	Electrolyte	GCD Conditions [a]	Initial Voltage Gap (V)	The Highest Power Density (mW cm^{-2})	Reference
K-DMO	6 M KOH and 0.2 M $Zn(Ac)_2$	5 mA cm^{-2}	0.66	139.9	This work
MnO_x/C-D	6 M KOH	-	-	138.0	3
MnO_2/Super	6 M KOH	-	-	127	4

P Li Co-EDM	-	1 mA cm^{-2} for discharge; 10 mA cm^{-2} for charge	1.04	-	5
Co/MnO@NC	6 M KOH and 0.2 M $Zn(Ac)_2$	20 mA cm^{-2}	0.82	146	9
Ni/MnO/CNF	6 M KOH and 0.2 M $Zn(Ac)_2$	10 mA cm^{-2}	0.93	138.6	10
LSM30	6 M KOH and 0.2 M $Zn(Ac)_2$	10 mA cm^{-2}	0.793	181.4	11

Reference

1. C. Han, J. Zhu, C. Zhi and H. Li, *J. Mater. Chem. A*, 2020, **8**, 15479-15512.
2. R. Cao, P. Zhang, Y. Liu and X. Zheng, *Appl. Surf. Sci.*, 2019, **495**, 143607.
3. N. Wang, W. Li, J. Liang, Y. Huang, Q. Cai, M. Hu, Y. Chen and Z. Shi, *J. Alloy. Compd.*, 2020, **846**, 156396.
4. Z. Huang, G. Li, Y. Huang, X. Gu, N. Wang, J. Liu, O. L. Li, H. Shao, Y. Yang and Z. Shi, *J. Power Sources*, 2020, **448**, 227385.
5. K. Fujimoto, Y. Ueda, D. Inohara, Y. Fujii and M. Nakayama, *Electrochim. Acta*, 2020, **354**, 136592.
6. J.-X. Zhang, L.-N. Zhou, J. Cheng, X. Yin, W.-T. Kuang and Y.-J. Li, *J. Mater. Chem. A*, 2019, **7**, 4699-4704.
7. J. A. Vigil, T. N. Lambert, J. Duay, C. J. Delker, T. E. Beechem and B. S. Swartzentruber, *ACS Appl. Mater. Interfaces*, 2018, **10**, 2040-2050.
8. Y. Li, S. Cao, L. Fan, J. Han, M. Wang and R. Guo, *J. Colloid Interface Sci.*, 2018, **527**, 241-250.
9. Y. Niu, X. Teng, S. Gong, X. Liu, M. Xu and Z. Chen, *Energy Storage Mater.*, 2021, **43**, 42-52.
10. D. Ji, J. Sun, L. Tian, A. Chinnappan, T. Zhang, W. A. D. M. Jayathilaka, R. Gosh, C. Baskar, Q. Zhang and S. Ramakrishna, *Adv. Funct. Mater.*, 2020, **30**, 1910568.
11. S. Yan, Y. Xue, S. Li, G. Shao and Z. Liu, *ACS Appl. Mater. Interfaces*, 2019, **11**, 25870-25881.